Assessment of an Innovative Way to Store Hydrogen in Vehicles

Andresa Baptista [1,*] **, Carlos Pinho** [2] **, Gustavo Pinto** [1] **, Leonardo Ribeiro** [1],
Joaquim Monteiro [1] **and Tiago Santos** [1]

1   ISEP—School of Engineering, Polytechnic of Porto, 4200-072 Porto, Portugal; gflp@isep.ipp.pt (G.P.);
    lsr@isep.ipp.pt (L.R.); jfmo@isep.ipp.pt (J.M.); 1130775@isep.ipp.pt (T.S.)
2   FEUP—Faculty of Engineering, University of Porto, 4200-465 Porto, Portugal; ctp@fe.up.pt
*   Correspondence: absa@isep.ipp.pt; Tel.: +351-228-340-500

Abstract: The use of hydrogen as an alternative to fossil fuels for vehicle propulsion is already a reality. However, due to its physical characteristics, storage is still a challenge. There is an innovative way, presented in this study, to store hydrogen in conventional vehicles propelled by spark-ignition reciprocating engines and fuel cells, using hydrogen as fuel; the storage of hydrogen will be at high pressure within small spheres randomly packed in a tank, like the conventional tank of fuel used nowadays in current vehicles. Therefore, the main purpose of the present study is to assess the performance of this storage system and compare it to others already applied by car manufacturers in their cars. In order to evaluate the performance of this storage system, some parameters were taken into account: The energy stored by volume and stored by weight, hydrogen leakage, and compliance with current standards. This system is safer than conventional storage systems since hydrogen is stored inside small spheres containing small amounts of hydrogen. Besides, its gravimetric energy density (GED) is threefold and the volumetric energy density (VED) is about half when compared with homologous values for conventional systems, and both exceed the targets set by the U.S. Department of Energy. Regarding the leakage of hydrogen, it complies with the European Standards, provided a suitable choice of materials and dimensions is made.

Keywords: energy storage system; hydrogen; permeation; packing factor; vehicle propulsion

1. Introduction

Some experts predict that, in the future, hydrogen will be used as a general-purpose energy vector, either for storing or transporting energy [1,2]. Major economies, like the Chinese, [3–5], German [6], and Japanese [7] economies, and that of the United States [8], among others, are about to boost the use of hydrogen, since their leaders are prone to establishing a friendly economic and political background. However, to achieve this goal, a great amount of work is still needed because there is a lack of infrastructure, namely refueling stations [9,10].

It is also possible to use an eventual surplus of renewable energy production from the wind, sun, and other sources to obtain hydrogen that can be stored until it is required by consumers [11]. In the cases of such surpluses, Tarkowski [12] studied the feasibility of underground hydrogen storage using salt caverns, deep aquifers, depleted gas fields, and depleted oil fields.

Specifically, there is a growing interest in the application of hydrogen for vehicle propulsion. Therefore, the storage of this fuel in a vehicle is of great importance. Indeed, almost 70% of publications in this scientific area are about the storage of hydrogen [11].

There are essentially two ways to store hydrogen [2]. The first way consists in storing hydrogen either as (i) compressed gas, or as a (ii) cryogenic liquid, or (iii) adsorbed in a metal, as a reversible

metal hydride, or (iv) even adsorbed in carbon nanofibers [2,13]. Alternatively, hydrogen is combined with certain chemical species, in order to get ammonia (NH_3), methanol (CH_3OH), etc. This issue is discussed at length elsewhere, so only a brief summary of it will be given here to allow the full assessment of the storage method for hydrogen studied in this paper.

It can be seen from Table 1 that hydrogen has a very low density, so, to get a large mass of hydrogen into a small container, the pressure of hydrogen in the container must be extremely high. Besides, hydrogen must be cooled down to −252.77 °C to liquefy, and even at such low temperatures its density is still very low, i.e., 77 kg m^{-3} [1,14].

Table 1. Basic chemical and physical data on hydrogen, methane, methanol, ethanol, and gasoline, adapted from [1,13].

Parameter	H_2	CH_4	CH_3OH	C_2H_5OH	Gasoline
Molecular weight (kg kmol^{-1})	2.016	16.04	32.04	46.06	107.0
Ignition temperature in air (°C)	585	540	385	423	230–480
Minimum ignition energy in air (MJ)	0.02	0.3	0.14	1.25	0.8
LHV (MJ kg^{-1})	119.9	50.0	19.9	27.7	44.0
Liquid density (kg m^{-3})	77	425	786	789	~751
Density at normal temperature and pressure (NTP) (kg m^{-3})	0.084	0.67	791	789	~751
Flammability limits in air (%)	4–77	4–16	6–36	4–19	1–7.6

Crowl and Jo [15] distinguish the hazards and risks connected with the use of hydrogen. Hazards stem from the flammable and explosive nature of the fuel, whereas risk is a mixture of the probability of an accident and the consequences of the accident. Anyway, a safety issue arises with the minimum ignition energy of hydrogen, which is very small compared with the homologous values for other gases—see Table 1 for some examples—which implies that the combustion of hydrogen can be easily triggered. Another safety issue of hydrogen relates to its large flammability range. Thus, it the build-up of the amount of hydrogen in confined spaces should be averted. Luckily, on the one hand, the high diffusivity of hydrogen facilitates the aeration of spaces, and, on the other hand, the low molecular weight of hydrogen promotes its upward dispersion, thus being difficult to find a point, in a given room, within the flammability range.

The present study is on an innovative way, proposed by Stenmark [16], to store hydrogen in conventional vehicles. Reciprocating internal combustion engines, gas turbines, or even fuel cells can propel these vehicles. The fuel, hydrogen, is stored at high pressure within small spheres randomly packed in a tank, like the conventional tank of fuel used nowadays in current vehicles.

The main purpose of the study is to assess the features of such a storage method regarding the energy stored per volume of the system (VED), energy stored per weight of the system (GED), leakage of hydrogen from the system, compliance with current standards, and comparison with other storage methods for hydrogen. According to Zhang et al. [2], for gaseous hydrogen stored at 700 daN cm^{-2}, which is the case for this storage method, the target established by the U.S. Department of Energy (US DoE) [17] for GED is 1.5 kWh kg^{-1} and for VED is 0.8 kWh L^{-1}.

2. Storage of Hydrogen

2.1. Compressed Gas

The most widespread storage method for hydrogen uses pressurized deposits, either man-made deposits or underground caves. According to Larminie and Dicks [13], the storage of hydrogen as a compressed gas has some advantages, namely (i) simplicity, (ii) unlimited storage time, and (iii) no purity requirements for hydrogen. In fact, such a storage method is the most commonly used for small amounts of hydrogen, and the hydrogen is stored within cylinders of various sizes and at various pressures. Moreover, there are suppliers scattered across Europe that are able to quickly deliver such cylinders.

The mass of H_2 per volume of storage tank at 293.15 K is 16 kg m^{-3} at 200 daN cm^{-2} and 24 kg m^{-3} at 300 daN cm^{-2}. Such low values are caused by the low density of H_2, even at high pressures. The same reason explains why the ratio of the mass of H_2 by the mass of both H_2 and the storage tank is seldom higher than 3% [18,19].

The material of the tank must be carefully chosen. Firstly, given that the molecule of H_2 is very small, its average velocity is very high. Thus, the permeation of H_2 through the walls of a containing tank is not negligible. Secondly, if the material of the tank is metallic, small bubbles of H_2 may appear entrapped within the walls of the tank with ensuing fissures on these walls. Finally, in tanks made of metallic alloys containing carbon, like steel, bubbles of CH_4 may appear, also entrapped within the walls of the tank, owing to a reaction between H_2 and carbon. As a result, the walls of the tank may crack, and such a phenomenon is the well-known hydrogen embrittlement. This hydrogen embrittlement can be averted with the addition of chromium and molybdenum to the steel [13,20,21].

A leak of H_2 from tanks at high pressure can be very harmful because such tanks may become jet-propelled missiles, and the H_2 leaked can auto ignite in quite a large range of flammability limits, generating an invisible flame, which worsens the problem. These hazards are tackled with relief valves, ruptures discs, and flame traps fitted on the tanks.

2.2. Liquid

Valenti [22] claims that, in view of the mobility based on hydrogen, the distribution and storage of liquid hydrogen, commonly designated as LH_2, is one of the most feasible options from energy, technical, and economic viewpoints. Liquid H_2 is stored at 22 K and, most of the time, below 5 daN cm^{-2}, as a cryogenic liquid within reinforced vacuum flasks, with capacities that can reach 3200 m^3, as is the case of a facility of National Aeronautics and Space Administration (NASA). Some car manufacturers have devoted great effort to research concerning the application of LH_2, as fuel, to internal combustion engines. The LH_2 is stored in cylindrical vacuum flasks, each with a capacity of 0.120 m^3, which corresponds to 9.2 kg of LH_2.

The rate of evaporation of H_2 inside the flasks depends on the thermal load (heat gains) on these flasks, which should be as low as possible. If the rate of evaporation of H_2 within the flask is higher than the H_2 consumption, then the pressure in the flask rises. The excess H_2 is either released to the atmosphere (small systems) or burnt in a flare stack (large systems). The pressure in the flask is kept constant through a relief valve and, as an extra safety device, a rupture disc is fitted to the flask to operate as a fuse sensible to pressure [1,13,23,24]. The mass of H_2 per volume of storage tank reaches 43 kg m^{-3} and the ratio of the mass of H_2 by the mass of both the H_2 and the storage flask reaches 14%. Explosive mixtures of H_2 and air in the storage flask must be avoided. Thus, prior to their filling with H_2, these flasks must contain nitrogen. According to Bossel et al. [25], the liquefaction of H_2 consumes at least 30 MJ kg^{-1}.

Finally, some hazards arise due to LH_2 being a cryogenic substance. Insulation must be applied over the surfaces of pipes and vessels containing LH_2, not only because contact with human skin and surfaces at such low temperatures is harmful to persons, but also to avoid liquefaction of the air with the subsequent formation of droplets of liquid air, which could cause explosion of nearby H_2.

2.3. Reversible Metal Hydride

There are metallic alloys of iron, nickel, chromium, and titanium, for example, that absorb H_2 through a reversible chemical reaction according the model of $A + H_2 \rightarrow AH_2$, with A being the absorbing alloy and AH_2 a metal hydride. The metallic alloy is within a container, normally a cylinder prepared to withstand pressures up to 30 daN cm^{-2}. The mass of H_2 per volume of storage tank depends on the alloy employed. Some of these values are shown in Table 2, and they are higher than the homologous values for the previously analyzed storage methods.

Table 2. Mass of H_2 per volume of container, adapted from [13].

Metallic Alloy	Chemical Formula	Mass of H_2 Per Unit Volume of Container (kg m^{-3})	Remarks
Aluminum hydride	AlH$_3$	140.8	Simple hydride. Performance poor.
Beryllium hydride	BeH$_2$	122.0	Simple hydride. Toxic. Performance poor.
Calcium hydride	CaH$_2$	90.1	Simple hydride. Performance poor.
Lithium borohydride	LiBH$_4$	123.5	Complex hydride. Toxic. Performance poor.
Palladium hydride	Pd$_2$H	50.0	Complex hydride. Expensive.
Titanium hydride	TiH$_2$	172.4	Simple hydride.
Titanium iron hydride	TiFeH$_2$	102.0	Complex hydride.

The filling of the container by H_2 occurs according to the reaction, $A + H_2 \rightarrow AH_2$, which is slightly exothermic, almost isobaric at pressures in the range of 1 up to 2 daN cm^{-2}, and takes only some minutes, depending on the capacity of the container. The cooling of the container is important to keep the pressure constant during the filling process; the refrigerant used is usually ambient air. At the end of the filling process, no absorbing alloy A remains to react, which is apparent because the pressure starts to increase, and so the container must be shut. When the H_2 stored in the container is required by a consumer, the reverse reaction of $A + H_2 \rightarrow AH_2$ must occur, i.e., the metal hydride is decomposed by $AH_2 \rightarrow A + H_2$, which, since this reaction is endothermic, is achieved by providing heat to the container, using either warm water or air.

The lifespan of these devices is such that the filling and discharge cycle can occur hundreds of times. However, the device can be prematurely damaged by excessive pressure during the filling process and by impurities in the hydrogen.

The superiority of this storage method of H_2 over the others relates to its low storage pressure; the system itself is safe when leakages occur from the container insofar as the temperature of the system drops in such cases, which stops the reaction of $AH_2 \rightarrow A + H_2$. The unwelcome features of this storage method of H_2 are mostly connected with its application in vehicles: Large volumes of containers for the normal autonomies required for cars; refilling times of nearly one hour for just 5 kg of H_2; the cooling and heating necessary for the filling and discharge processes; and the high purity required for H_2 to prevent damage to the system.

2.4. Carbon Nanofibers

Amorphous carbon, activated carbon, and graphite have been used, since a long time ago, to absorb some substances. Unfortunately, these materials are ineffective for storing hydrogen.

The target set by the Department of Energy of the USA for hydrogen storage with carbon nanofibers applied in vehicles propelled by fuel cells is 62 kg of H_2 per cubic meter of absorbent material and the percentage weight of stored H_2 to the total system weight is 5.5% [26].

Nowadays, for H_2 storage, essentially three types of carbon nanofibers are objects of interest, namely: Graphitic nanofibers, single-walled nanotubes (SWNT), and multi-walled nanotubes (MWNT). The absorption of H_2 by MWNT can reach 5% (weight of stored H_2 to the total system weight) [27].

3. Method of Assessment of the Proposed Storage System

As aforementioned, the present study is on an innovative way to store hydrogen in conventional vehicles to assess the performance of the storage system implied, and the methodology followed is summarized in Table 3.

Table 3. Methodology followed to assess the performance of an innovative way to store hydrogen.

Methodology Summary	
Step 1	Description of the storage system
Step 2	Gravimetric energy density (GED), volumetric energy density (VED)
Step 3	Selection of materials for the sphere and permeation
Step 4	Safety factor (CS)
Step 5	Packing factor (PF)

3.1. Description of the Storage System (Step 1)

The aim of the innovative system studied in this paper is the feeding of internal combustion engines applied in automotive propulsion. Accordingly, the design of this system has three primary goals, namely, the improvement of (i) the ratio of the weight of stored H_2 to the total system weight and (ii) of the ratio of the weight of stored H_2 to the total system volume, and (iii) to instill confidence in the user.

The system consists of a set of loosely packed small spheres enclosed within a tank, which itself can take any shape, as shown in Figure 1. Hydrogen is contained in the small spheres, at atmospheric temperature and high pressure; the pressure can reach a peak of 700 daN cm^{-2}. Each sphere has embedded a microchip, a rectangular parallelepiped solid ($0.5 \times 0.5 \times 2.5$ mm), that controls either the charge or discharge of the sphere by hydrogen. If the outside pressure surrounding the spheres, which is the pressure of hydrogen in the tank, is bellow a given value, say 5 daN cm^{-2}, then the outward flow of hydrogen from the spheres is halted by the microchip; otherwise, the spheres will leak, in a controlled way, hydrogen to be used by the consumer.
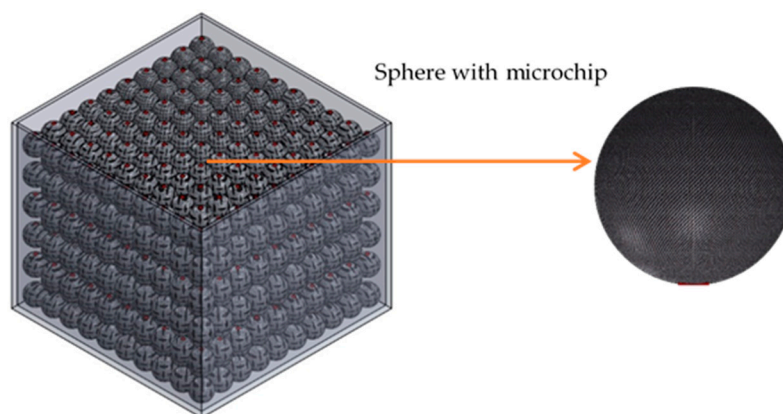
Figure 1. New system for hydrogen storage.

3.2. GED and VED (Step 2)

The performance of the system was assessed through both the gravimetric and volumetric densities. The gravimetric energy density (GED) is the ratio of energy of hydrogen stored in a sphere by the total weight of hydrogen plus the sphere. The volumetric energy density (VED) is the ratio of energy of hydrogen stored in a sphere by the outer volume of the sphere. For a given inner diameter of a sphere, the energy of the hydrogen contained in the sphere is calculated through Equation (1):

$$E_{sph} = m_{H_2} LHV_{H_2}, \qquad (1)$$

where LHV_{H_2} is given in Table 1, and the mass of hydrogen within a sphere, m_{H_2}, is calculated by Equation (2):

$$m_{H_2} = \frac{P \cdot V_{in\ sph}}{Z \cdot R_{H_2} \cdot T_{H_2}}. \qquad (2)$$

R_{H_2} is the ideal gas hydrogen constant, taken as 4124 J kg^{-1} K^{-1}; T_{H_2} is the temperature of hydrogen, assumed as 293.15 K; and Z is the compressibility factor of hydrogen at 700 daN cm^{-2} and 293.15 K, taken as 1.46 [28].

According to the above definitions, the gravimetric density is, as shown by Equation (3):

$$GED_{sph} = \frac{E_{sph}}{m_{sph}}, \tag{3}$$

and the volumetric density is, as shown by Equation (4):

$$VED_{sph} = \frac{E_{sph}}{V_{out\ sph}}. \tag{4}$$

3.3. Selection of Materials and Permeation (Step 3)

Materials with high strength, such as steel, high magnesium-steel, aluminum alloys, titanium, magnesium, and magnesium alloys, are susceptible to hydrogen embrittlement, mostly at elevated temperatures, pressures, and exposure times [29].

Initially, the sphere was considered to be made of one single material. The set of materials studied for the sphere is referred to in Table 4, as well as their most relevant properties connected with the current study. Silicon (Si) was considered only for the microchip.

Table 4. Properties of the studied materials.

Material	P_o		P_o Reference	ϱ (kgm^{-3})	σ_{yield} (MPa)	σ_{str} (MPa)
CFEP	1.9×10^{-16}	mol/(msPa)	[30]	1790	-	4000
Al 5050-H38	4.34×10^{-20}	mol/(msPa$^{0.5}$)	[31]	2697	220	-
HDPE	8.98×10^{-16}	mol/(msPa)	[30]	1275	-	27
SS316	1.13×10^{-18}	mol/(msPa$^{0.5}$)	[32]	7990	290	-
SS403	1.44×10^{-15}	mol/(msPa$^{0.5}$)	[33]	7800	310	-
Inconel 600	3.72×10^{-18}	mol/(msPa$^{0.5}$)	[32]	8470	550	-
Inconel 718	1.13×10^{-17}	mol/(msPa$^{0.5}$)	[32]	8190	1100	-
GFRP	4.6×10^{-17}	mol/(msPa)	[34]	875	-	552
Ti	8.13×10^{-14}	mol/(msPa$^{0.5}$)	[35]	4630	1084	-
W	4.94×10^{-32}	mol/(msPa$^{0.5}$)	[36]	12,750	1045	-
Si	1×10^{-8}	mol/(m^{2}sPa$^{0.5}$)	[37]	3220	-	-

The permeation of hydrogen through solid surfaces can be significant, which creates safety hazards since the leaking of hydrogen from within a pressurized tank to the outside can generate an explosion. The values of permeation are given in some bibliographic sources, but are associated with great uncertainties, and are not always expressed in the same units. Po stands for the value of permeation at 293.15 K and 101.3 kPa.

The tensile test diagram (elongations plotted along the horizontal axis and the corresponding stresses given by the ordinates) of the metallic materials of Table 4 show a noticeable yielding stress, σ_{yield}, whereas for the polymeric and composite materials of Table 4, only the fracture stress, σ_{str}, is shown.

From Table 4, it follows that the metallic alloys (Al 5050-H38, SS316, SS403, Inconel 600, Inconel 718, Ti, W) have lower values of permeation, but higher values of strength than the polymeric materials (high-density polyethylene, HDPE). Besides, the composite materials (carbon fiber epoxy, CFEP; glass fiber reinforced polymer, GFRP) have higher values of permeation and either equal or higher values of strength than the metallic alloys.

These considerations also suggest the study of spheres made of two materials, i.e., two concentric spherical layers: The inner layer, called the liner, to provide resistance to the permeation of hydrogen and, accordingly, Al5050-H38 was adopted for this layer; the outer layer, called the structural layer,

to provide strength, and so CFEP was adopted. The materials considered for the microchip were either Si or SS316, because they are both already used in small electronic devices owing to their easy tooling capacities [16].

Hydrogen leaks from a sphere by two ways: By permeation across the wall of the sphere, and through the interfaces microchip/spheres. The mole flowrate of hydrogen through the wall of a sphere made of two layers was calculated with the Equation (5):

$$\dot{N}_{H_2\,sph} = \frac{x_{sph} - x_{out}}{\frac{1}{4\pi P_{o\,liner-corrected}}\left(\frac{1}{r_{i\,liner}} - \frac{1}{r_{o\,liner}}\right) + \frac{1}{4\pi P_{o\,stru-corrected}}\left(\frac{1}{r_{i\,strut}} - \frac{1}{r_{e\,strut}}\right)}. \tag{5}$$

In Equation (5), the resistance to permeation at the interface of the two layers is neglected, which is a conservative assumption that overestimates the flowrate of hydrogen permeation from the spheres. Besides, the corrected values of permeation corrected used in Equation (5), either for the liner or the structural layer, must be expressed in mol m^{-1} s^{-1}. If Po is given in mol m^{-1} s^{-1} Pa^{-1}, then the value of the corrected permeation is calculated with Po times the pressure within the sphere; if Po is in mol m^{-1} s^{-1} Pa$^{-0.5}$, then the value of permeation corrected is calculated with Po times the square of the pressure within the sphere. Finally, for Po in mol m^{-2} s^{-1} Pa$^{-0.5}$, the value of corrected permeation is Po times the inner radius of the sphere and times the square of the pressure within the sphere. The value of the corrected value of permeation for the outer or structural layer was calculated assuming this layer is subjected to the same pressure as the inner layer, which again overestimates the flowrate of hydrogen permeation from the spheres. Overestimating the flowrate of permeation of hydrogen was a precautionary measure to avoid or mitigate hazards.

This flowrate of permeation through the microchip is, as shown by Equation (6):

$$\dot{N}_{H_2\,microchip} = Po\cdot0.5\cdot0.5\cdot P^{1/2}. \tag{6}$$

The total mole flowrate of hydrogen through a sphere with the microchip incorporated is the sum of the values of Equations (5) and (6); it increases with the inner pressure/temperature and aging of the spheres.

The EU 406 regulation [38] concerns the technical approval of vehicles fueled by hydrogen contained within metallic or non-metallic reservoirs. The permeation flowrate can be neglected for metallic reservoirs (type 1, 2, and 3). Reservoirs made of polymeric materials (type 4) must be subjected to permeation tests. In fact, polymeric materials have much higher permeability than metallic materials [39]. Moreover, the same regulation allows a maximum permeation flowrate of 6 Ncm^3 h^{-1} L^{-1} (NPT) per liter of inner volume of the reservoir at steady state. This value is proposed in order to prevent inflammable mixtures of hydrogen and air in spaces, such as garages, for example, assuming the minimum air renovations per hour as 0.03 [40].

Temperature also affects the permeation of hydrogen through walls [41]. It is likely that in the currently studied system temperature peaks of up to 85 °C can occur during the fast filling of spheres, but it is expected that temperatures below 50 °C will be normal. As the aforementioned tests will be performed at temperatures below 55 °C, it is necessary to use a correction factor to obtain the permeation flowrate at temperatures other than the test temperature from the experimentally obtained flowrate, [39,42].

As time goes by, the ability of a reservoir to hinder the permeation of hydrogen drops, i.e., the permeation value of its material, increases, but this phenomenon is not yet fully understood and, accordingly, an aging factor of 2 is assumed [39]. Returning to the present case, the value of hydrogen concentration, $C_\%$, see Equation (7), must be under 1%; $C_\%$ is the ratio of the flowrate of hydrogen that leaves, by permeation, the envelope tank, Q_g, and the sum of Q_g with the flowrate of air into the space owing to air renovation, Q_a:

$$C_\% = \frac{100\cdot Q_g}{Q_a + Q_g}, \tag{7}$$

then, Q_{px}, see Equation (8), is the maximum flowrate of the permeation of hydrogen:

$$Q_{px} = \frac{Q_a \cdot C_\%}{100 - C_\%} \cdot \frac{60 \times 10^6}{V_{int\ res} \cdot f_a \cdot f_t}, \tag{8}$$

where $V_{int\ res}$ is the inner volume of each sphere, fa is the aging factor of 2, and ft is the factor of correction for the temperature.

3.4. Safety Factor (Step 4)

Equation (9) was used to size the structural spherical layer with a thin wall ($\frac{t}{r} \ll 1$):

$$t_{outer} = \frac{P \cdot r}{2 \cdot \sigma_{outer}} \cdot CS, \tag{9}$$

where t is the thickness and r is the radius of the shell. The ISO 11119-3 standard [43] recommends the use of a safety factor, CS, in the range of 2 up to 3 for conventional reservoirs of carbon fiber.

The currently studied storage system is composed of many small spheres, each containing small amounts of hydrogen (below 3 g) and, accordingly, the plausibility of a safety factor lower than 2, which will entail higher values of both VED and GED of the system. In fact, a report from Echtermeyer and Lasn [44] proposes, based on the DNV-OS-C501 standard [45], new values of CS for sizing reservoirs made of composite materials and used for the storage and/or transport of hydrogen. Moreover, this report states that CS must guarantee the safety of the spheres, which is equated to stating that the hazard ensuing from the use of these spheres has to be socially acceptable. The report assesses the hazard acceptability with Table 5 that contains annual probabilities of failure according to nautical and aeronautical industries, as a function of the number of casualties or deaths.

Table 5. Annual probabilities of failure according to nautical and aeronautical industries, adapted from [44].

Number of Casualties	Probability of Annual Failure
<10	10^{-5} to 10^{-6}
<100	10^{-7} up to 10^{-8}
<1000	10^{-9}, unacceptable

According to Echtermeyer and Lasn [44], it is sound practice to use a probability of annual failure inferior to 10^{-6} for sizing pressurized reservoirs applied to vehicles, which corresponds to a number of casualties less than 10. The volume or mass of hydrogen transported corresponds, for the currently studied case, to just one sphere. This implies that in the case of the bursting of one sphere, the other spheres can be slightly affected, but not torn apart, and the amount of hydrogen released is the hydrogen contained in just one sphere.

Table 6 shows estimations of the consequences of accidents and of the acceptable annual probabilities of failure, depending on the amount of hydrogen transported and the demographic density.

Echtermeyer and Lasn [44] also advise, following Table 6, that the maximum amount of hydrogen to be transported must not exceed 1000 kg across scarcely populated areas, and 350 kg across densely populated areas. Following Tables 5 and 6, these authors created safety classes with the purpose of defining a CS suitable for a given application, see Table 7.

Table 8 presents values of CS given by the authors for brittle fracture, depending on the safety class and the coefficient of variation of the material (CoV), provided that, in the case of impact, it will not be sustained by the spheres (in the current case, the impact must be sustained by the enclosing tank). The CoV is a factor related with the composite material of the spheres and takes into account the variation of the properties of such material (angles and properties of fibers) [44].

Table 6. Estimations of the consequences of accidents and of the acceptable annual probabilities of failure, adapted from [44].

H$_2$ Mass (kg)	Reach of the Explosion (m)	Scarcely Populated		Densely Populated	
		No. Casualties	Probability of Annual Failure	No. Casualties	Probability of Annual Failure
100	10	6	9.3×10^{-6}	16	5.2×10^{-7}
350	35	21	2.2×10^{-7}	192	2.8×10^{-10}
500	50	30	7.4×10^{-8}	393	3.3×10^{-11}
700	70	42	2.7×10^{-8}	770	4.4×10^{-12}
1000	100	60	9.3×10^{-9}	1571	5.2×10^{-13}

Table 7. Safety classes depending on the probability of annual failure, adapted from [44].

Type of Fracture	Safety Class				
	Low	Normal	High 1	High 2	High 3
Ductile	10^{-3}	10^{-4}	10^{-5}	-	-
Brittle	10^{-4}	10^{-5}	10^{-6}	10^{-7}	10^{-8}

Table 8. Values of CS for brittle fracture, depending on the safety class and CoV of the material of the spheres, adapted from [44].

Safety Class	CoV < 5%	CoV = 10%	CoV = 12.5%	CoV = 15%
Low	1.11	1.28	1.41	1.60
Normal	1.15	1.40	1.62	1.96
High 1	1.18	1.53	1.86	2.46
High 2	1.22	1.67	2.16	3.21
High 3	1.25	1.83	2.53	4.46

In the currently studied storage system, as the total amount of hydrogen contained in the system is under 5 kg and as each sphere contains less than 3 g of hydrogen, it is thus plausible to assume the low safety class. Besides, the CoV can be assumed as 12.5%, which is a conservative estimation. Then, the resulting CS can be taken as 1.41.

Figure 2 represents a sphere composed of two materials with a microchip embedded. The materials considered for the microchip were Si and SS316. The shape of the microchip was considered as solid parallelepiped, neglecting the channels in it to control the charge and discharge of the sphere, ($0.5 \times 0.5 \times 2.5$ mm). The strength calculations of the spheres did not take into account the microchip.
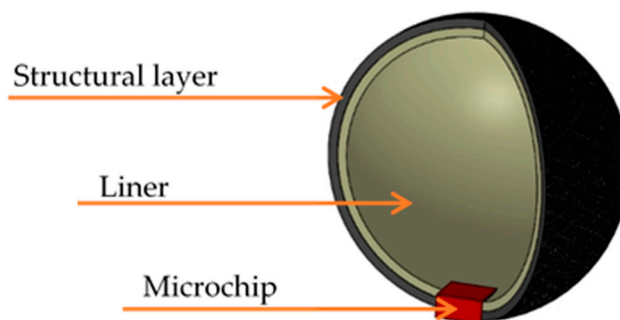
**Figure 2.** Sphere with microchip.

3.5. Packing Factor (Step 5)

It is paramount to increase, as much as possible, the number of spheres in the envelope tank. Aigueperse et al. [46] found that equal spheres thrown into a reservoir are likely to occupy the space

according to arrangements like crystalline structures. The simplest arrangement of spheres is shown in Figure 3 and is known as a body centered cubic (BCC) structure. Here, (a) indicates the position of the spheres' centers, whereas at (b), the spheres are shown in the lattice. The packing factor, PF, of the BCC is approximately 0.52.

(a)   (b)
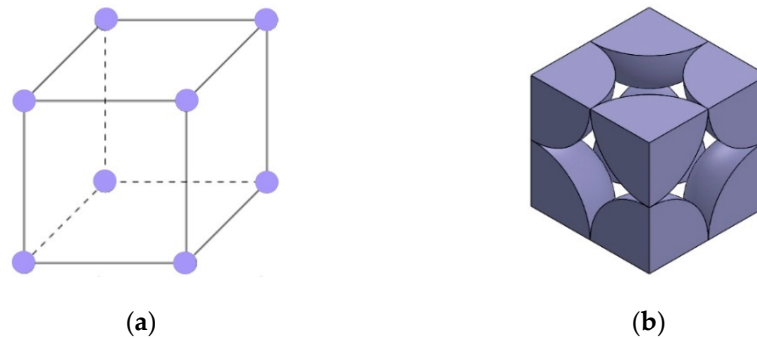
Figure 3. BCC with spheres. (**a**) Position of the centers of spheres; (**b**) Structure.

According to a conjecture presented by Kepler at 1611 (one of David Hilbert problems), no three-dimensional arrangement of spheres has a higher PF than the hexagonal close packing (HCP) [47], see Figure 4, where (a) indicates the position of the spheres' centers, and at (b), the spheres are shown in the lattice. The corresponding PF is approximately 0.74. In 1998, Thomas Hales presented a proof of the conjecture of Kepler, assisted by a computer program named proof assistant, Isabelle theorem prover HOL Light®, and such proof was finally accepted in 2017 [48]. As shown in Figure 4b, the diagonal of each face of the cube is two times the diameter of the spheres.

(a)   (b)
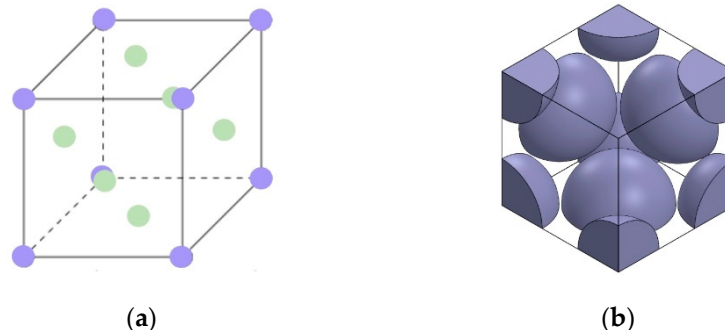
Figure 4. HCP structure. (**a**) Position of the centers of spheres; (**b**) Structure.

Despite the afore-mentioned assumption of Aigueperse et al. [46], there is, in fact, no way to guarantee a given lattice for the arrangement of spheres thrown into a reservoir. At this juncture, it is necessary to distinguish the packing randomly compact (PRC) and the packing randomly loose (PRL) arrangement.

The PRC is the most compact possible arrangement for spheres randomly thrown into a reservoir and is only achievable with vibration of the reservoir [49]. Numerous experimental studies indicate values of PF converge towards 0.64 [50]. To the PRL, the value of PF is generally taken as 0.60 [50]. Onoda et al. [51] obtained a PF of 0.555 for spheres of glass immersed in a liquid, in a situation of negligible gravitational force. It must be said that PRC and PRL are modes of packing not fully understood yet, and what is known was obtained mostly through experimentation [50]. In Table 9, some values of PF obtained by several authors are given.

Pouliquen et al. [56] concluded that the speed at which the spheres are introduced into a reservoir varies inversely with the resulting PF; the minimum PF obtained was 0.62. Donev [54] obtained a PF equal to 0.625 with a cubic reservoir filled with spheres of a diameter equal to 3.175 mm. Computational

simulations have shown that ellipsoids with ratios between great and small diameters in the range of 1.2 up to 1.3 can be accommodated with a PF equal to 0.73. Man et al. [55] have shown experimentally that the packing factor can reach 0.642 with glass spheres of an 11 mm diameter contained in a spherical reservoir, in which spheres were dumped randomly into the reservoir while it was manually shaken and isopropanol was used as a lubricant.

Table 9. Values of PF for several situations.

| PF	Reservoir	Vibration	Lubricant	Material of Spheres	Reference
0.575	Cylinder	No	No	Nylon	[52]
0.582	Cylinder	No	No	Steel	[53]
0.594	Sphere	No	No	Steel	[53]
0.605	Cylinder	No	No	Plexiglass	[52]
0.608	Cylinder	No	No	Steel	[52]
0.611	Cylinder	No	Oil	Steel	[52]
0.617	Cylinder	Yes	No	Steel	[53]
0.625	Cube	Yes	No	Steel	[54]
0.629	Cylinder	Yes	No	Nylon	[52]
0.634	Sphere	Yes	No	Steel	[52]
0.635	Sphere	Yes	No	Steel	[52]
0.636	Cylinder	Yes	Oil	Steel	[52]
0.636	Cylinder	Yes	No	Plexiglass	[52]
0.638	Cylinder	Yes	No	Steel	[52]
0.642	Sphere	Yes	Isopropanol	Glass	[55]
0.670	Cube	Yes	No	Steel	[56]

4. Results

Figure 5 shows the GED evaluated with Equation (3). For a determined pressure and ID, the energy of the hydrogen contained within a sphere has a value given by Equation (1). Besides, the GED increases as materials with higher strength are used to make the spheres (and so the weight of the spheres drops). The gains of GED obtained using materials with a higher strength increase with the ID (GED is proportional to the cubic of ID). As can be seen in Figure 5, for composite materials (CFEP and GFRP), values of GED are 3 to 8 times higher than for both polymeric and metallic materials.
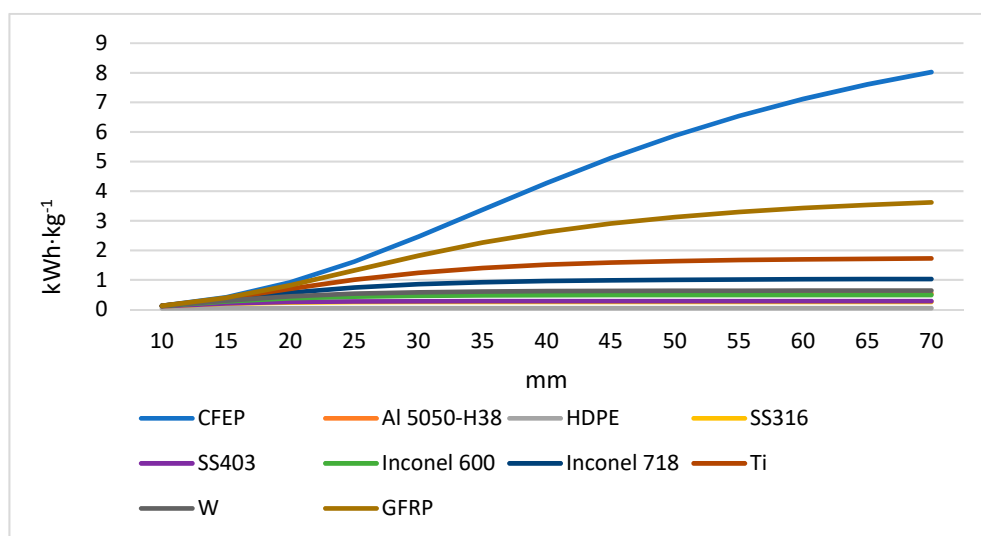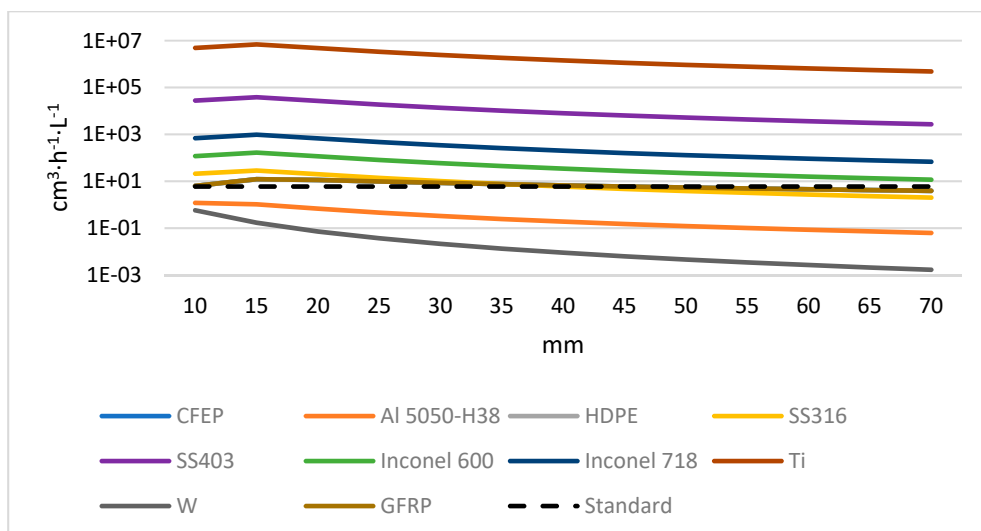

Figure 5. GED of spheres made of several materials with ID from 10 up to 70 mm, at 700 daN cm^{-2} of inside pressure.

Figure 6 shows the VED calculated with Equation (4). For a determined pressure and ID (and so of a given value of energy within a sphere), the VED increases as spheres are made of materials with higher strength (volume of the spheres drops). As can be seen in Figure 6, composite materials (CFEP and GFRP) have the best values of VED (lowest values of the thickness of spheres).
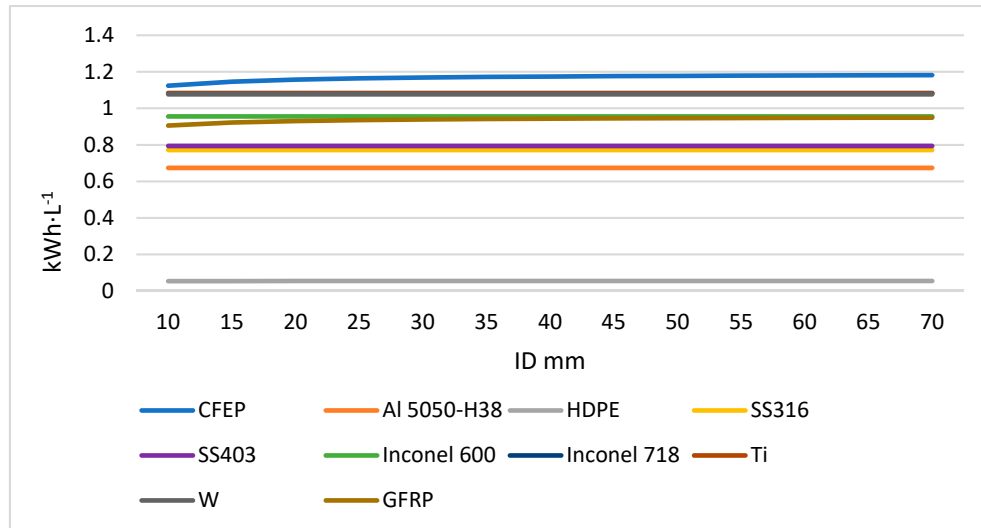

Figure 6. VED of spheres made of several materials with ID from 10 up to 70 mm, at 700 daN cm^{-2} of inside pressure.

Figure 7 shows the permeation flowrate calculated with Equation (5), considering that there is no microchip and the sphere is made of just one material. As expected, the graph shows that the leaks through permeation are lowest for spheres made with metallic materials, like Al and W, as shown by the values of permeation in Table 4. Besides, as the volume (or the ID) of the sphere increases, then its thickness also increases, see Equation (9), which explains the decreasing of the permeation flowrate with increasing ID.


Figure 7. Flowrate of permeation for spheres made of several materials with ID from 10 mm and up to 70 mm, at 700 daN cm^{-2} of inside pressure.

Figure 8 shows the mass of one sphere of CFEP, with microchip included, made of either SS316 or Si, for ID from 10 to 70 mm, at 700 daN cm^{-2} of inside pressure.
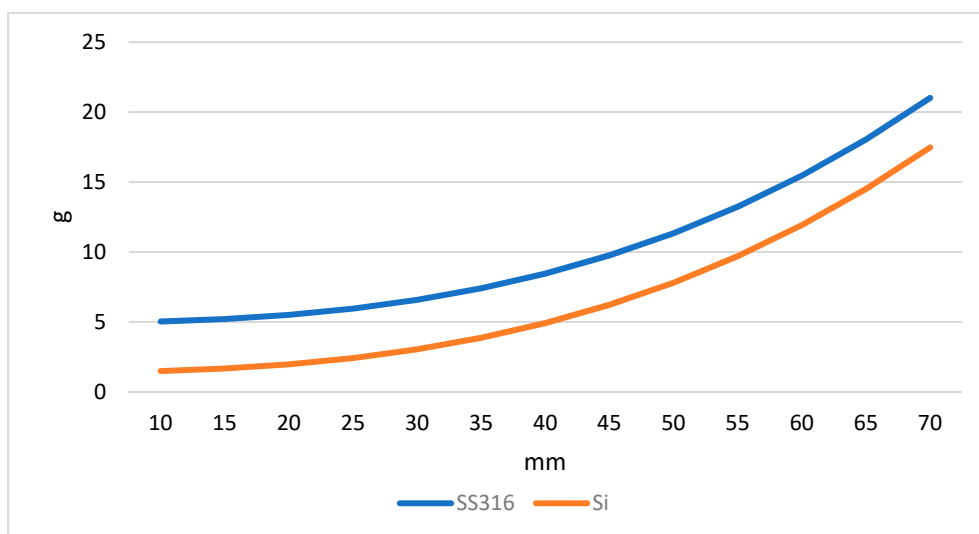
Figure 8. Mass of one sphere of CFEP, with microchip included, made of either SS316 or Si, for ID from 10 to 70 mm, at 700 daN cm^{-2} of inside pressure.

Figure 9 shows a comparison of the values of GED for spheres made of CFEP, with a microchip inserted, made of either SS316 or S. The explanation of both curves is like the explanation of the curves of Figure 5.
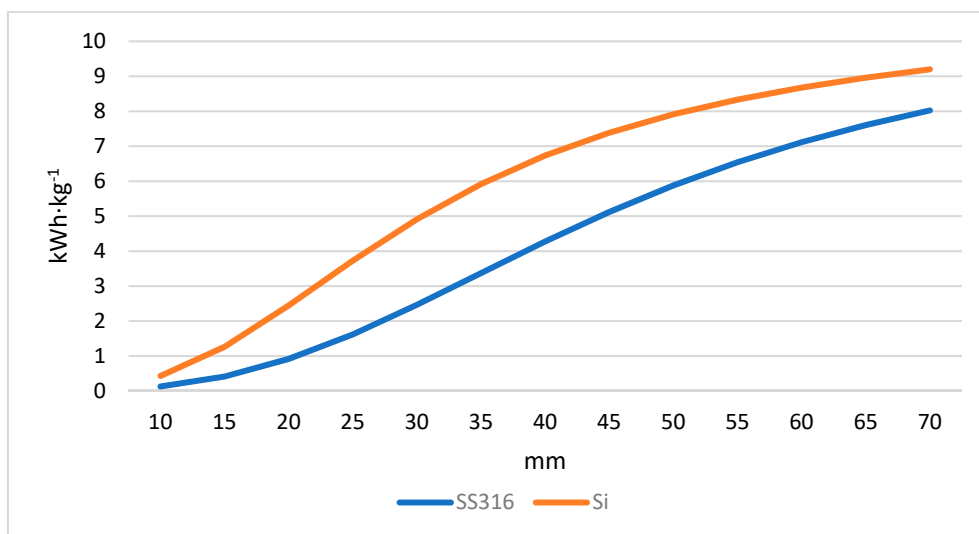
Figure 9. GED for spheres made of CFEP, equipped with a microchip, made of either SS316 or Si, for ID from 10 to 70 mm, at 700 daN cm^{-2} of inside pressure.

According to Figure 10, which shows the total permeation value (across the sphere and across the microchip), it is clear that the permeation across the sphere is almost negligible when compared with the permeation across the microchip. Thus, it is plausible to consider that the permeation value across the microchip is the total permeation. It is also noted that the sphere with the microchip of Si does not comply with the limit that is established by the European Standard (6 cm^3 h^{-1} L^{-1}, see dashed line). In the case of the sphere with a microchip of SS316, only the spheres with an ID higher than 45 mm comply with the standard.
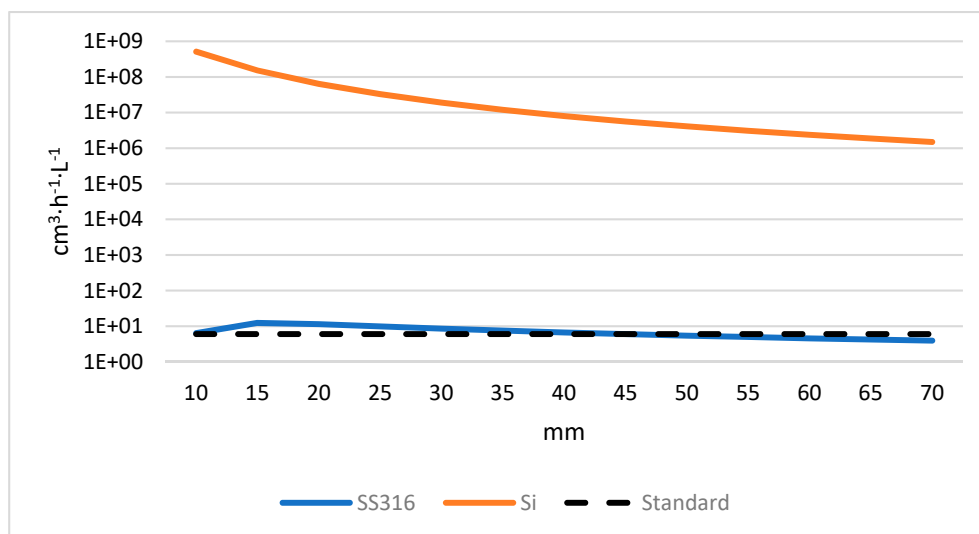
Figure 10. Permeation for spheres made of CFEP, equipped with a microchip, made of either SS316 or Si, for ID from 10 to 70 mm, at 700 daN cm^{-2} of inside pressure.

Table 10 presents the major characteristics of the complete storage system (storage tank + spheres), using spheres with an ID of 70 mm, a packing factor between 0.52 and 0.74, a safety factor of 1.41, and a 0.122 m^3 internal volume tank for the two types of microchip material.

Figures 11 and 12 show the comparison between the system under study and two actual road vehicles: Toyota Mirai and Hyundai Nexo. The GED of the sphere system is about 3 times higher than the GED for the vehicles mentioned because the total mass of the system is only 15% to 20% of their mass storage system. On the other hand, the VED and the total mass of H$_2$ stored is only about 50%, making these indicators a major disadvantage of the system studied against the actual hydrogen propulsion road vehicles. Regarding the Mirai and Nexo vehicles, the values shown are provided by the manufacturers. The values of the system under study have a range bar due to several values being adopted to the packaging factor and the density of the chip material [57,58].
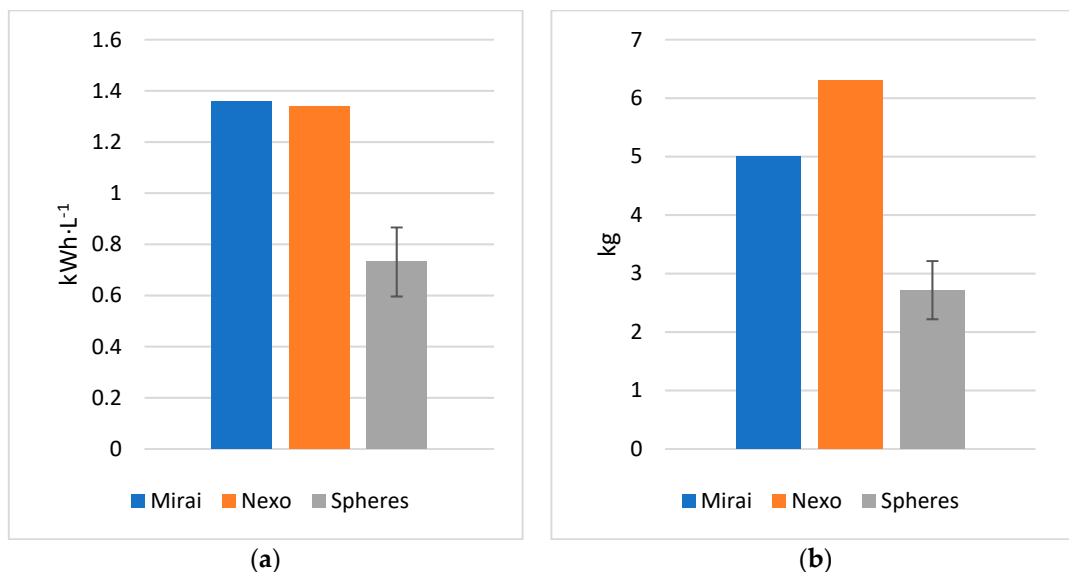

(**a**) (**b**)
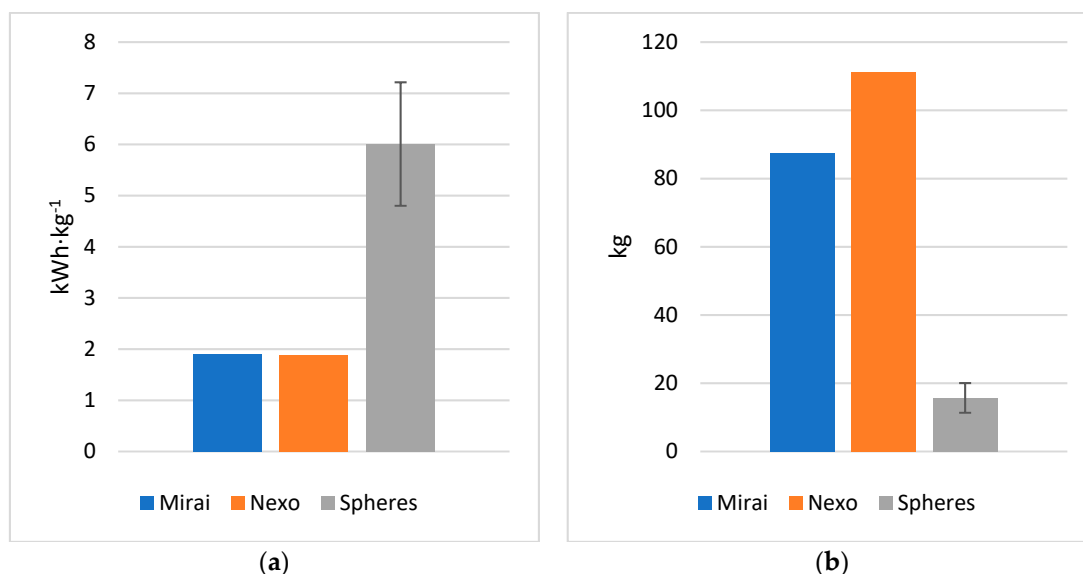
Figure 11. Comparison between the system under study and the storage systems of Toyota Mirai and Hyundai Nexo, regarding the (**a**) GED and (**b**) total system mass.

Table 10. Characteristics of the storage system (storage tank + spheres), using different packaging factors, CS 1.41.

Microchip Material	SS316				Si			
Packaging factor	**0.52**	**0.60**	**0.63**	**0.74**	**0.52**	**0.60**	**0.63**	**0.74**
Number of spheres	338	390	410	482	338	390	410	482
GED_{syst} (kWh kg^{-1})	5.98	6.20	6.27	6.48	6.62	6.87	6.96	7.22
VED_{syst} (kWh L^{-1})	0.61	0.70	0.74	0.87	0.61	0.70	0.74	0.87
Mass of the system (kg)	12.54	13.98	14.53	16.52	11.34	12.60	13.08	14.82
Mass of H_2 (kg)	2.25	2.60	2.73	3.21	2.25	2.60	2.73	3.21

(**a**)

(**b**)

Figure 12. Comparison between the system under study and the storage systems of Toyota Mirai and Hyundai Nexo, regarding the (**a**) VED and (**b**) the mass of stored hydrogen.

5. Conclusions

The hydrogen storage system studied in this paper is safer than the conventional systems for the same purpose, since the mass of hydrogen is divided, as required, in several small spheres containing nonhazardous amounts of fuel. The chief advantage of this system, when compared with systems already adopted by car manufacturers, is its GED, whereas it performs not so well in terms of VED. It exceeds the target set by the US DoE of GED = 1.5 kWh kg^{-1} and of VED = 0.8 kWh L^{-1}. Moreover, both GED and VED increase with increasing internal diameters of spheres.

The leakage across spheres is negligible when compared with the leakage across the microchip. However, it must be stressed that, regarding leakage, not all materials are suitable for the construction of the microchip, namely Si.

The packing factor must be as high as possible to increase the GED and VED, which is achievable through vibration, lubrication, the speed at which the spheres are introduced into the envelope tank, and the possibility of using spheres with different diameters.

Beyond the scope of the present study was the charge and the discharge of the envelope tank, with which arise new challenges, at the fuel stations, a matter that still needs to be solved.

Author Contributions: The authors have made equivalent contributions.

Abbreviations

List of Symbols

C	Concentration
CS	Safety factor
E	Energy
fa	Aging factor
ft	Correction factor for the temperature
GED	Gravimetric energy density
LHV	Lower heating value
m	Mass
$\dot{N}$	Permeation molar flowrate
P	Pressure
Po	Permeation at NTP
Q	Flowrate
R	Gas constant
r	Radius
T	Temperature
t	Thickness
V	Volume
VED	Volumetric energy density
Z	Compressibility factor

Subscripts

a	Air into the space owing renovation
g	Hydrogen leaves envelope tank
in sph	Internal sphere
int res	Inner volume sphere
Out sph	Outer sphere
px	Maximum hydrogen permeation
sph	Sphere
str	Strength
struc	Structural
yield	Yield

Greek symbols

ϱ	Density
σ	Stress

References

1. Spiegel, C. *Designing and Building Fuel Cells*, 1st ed.; McGraw-Hill: New York, NY, USA, 2007; ISBN-13: 978-0071489775.
2. Zhang, F.; Zhao, P.; Niu, M.; Maddy, J. The survey of key technologies in hydrogen energy storage. *Int. J. Hydrogen Energy* **2016**, *41*, 14535–14552. [CrossRef]
3. Ren, J.; Gao, S.; Tan, S.; Dong, L. Hydrogen economy in China: Strengths–weaknesses–opportunities–threats analysis and strategies prioritization. *Renew. Sustain. Energy Rev.* **2015**, *41*, 1230–1243. [CrossRef]
4. Ren, J.; Gao, S.; Tan, S.; Dong, L.; Scipioni, A.; Mazzi, A. Role prioritization of hydrogen production technologies for promoting hydrogen economy in the current state of China. *Renew. Sustain. Energy Rev.* **2015**, *41*, 1217–1229. [CrossRef]
5. Lu, J.; Zahedi, A.; Yang, C.; Wang, M.; Peng, B. Building the hydrogen economy in China: Drivers, resources and technologies. *Renew. Sustain. Energy* **2013**, *23*, 543–556. [CrossRef]
6. Ball, M.; Wietschel, M.; Rentz, O. Integration of a hydrogen economy into the German energy system: An optimising modelling approach. *Int. J. Hydrogen Energy* **2007**, *32*, 1355–1368. [CrossRef]
7. Lee, D.-H. Development and environmental impact of hydrogen supply chain in Japan: Assessment by the CGELCA method in Japan with a discussion of the importance of the importance of biohydrogen. *Int. J. Hydrogen Energy* **2014**, *39*, 19294–19310. [CrossRef]

8.　Lattin, W.; Utgikar, V. Transition to hydrogen economy in the United States: A 2006 status report. *Int. J. Hydrogen Energy* **2007**, *32*, 3230–3237. [CrossRef]

9.　Europe Hydrogen Refuelling Infrastructure. Available online: https://h2me.eu/about/hydrogen-refuelling-infrastructure/ (accessed on 11 April 2019).

10.　USA Hydrogen Refuelling Infrastructure. Available online: https://afdc.energy.gov/fuels/hydrogen_locations.html#/find/nearest?fuel=HY (accessed on 11 April 2019).

11.　Fonseca, J.D.; Camargo, M.; Commenge, J.-M.; Falk, L.; Gil, I.D. Trends in design of distributed energy systems using hydrogen as energy vector: A systematic literature review. *Int. J. Hydrogen Energy* **2019**, *44*, 9486–9504. [CrossRef]

12.　Tarkowski, R. Underground hydrogen storage: Characteristics and prospects. *Renew. Sustain. Energy Rev.* **2019**, *105*, 86–94. [CrossRef]

13.　Larminie, J.; Dicks, A. *Fuel Cell Systems Explained*, 2nd ed.; John Wiley & Sons, Ltd.: West Sussex, UK, 2003; ISBN-13: 978-0768012590.

14.　Aceves, S.M.; Berry, G.D.; Martinez-Frias, J.; Espinosa-Loza, F. Vehicular storage of hydrogen in insulated pressure vessels. *Int. J. Hydrogen Energy* **2006**, *31*, 2274–2283. [CrossRef]

15.　Stenmark, L.; Uppsala University, Uppsala, Sweden. Personal communication, 2010.

16.　Crowl, A.; Jo, Y. The hazards and risks of hydrogen. *J. Loss Prev. Process Ind.* **2007**, *20*, 158–164. [CrossRef]

17.　Stetson, N.T. Hydrogen storage overview. In Proceedings of the DoE Annual Merit Review and Peer Evaluation Meeting, Washington, DC, USA, 16–20 June 2014.

18.　Vieira, A.C.; Faria, H.; Oliveira, R.; Correia, N.; Marques, A.T. High Pressure On-board Storage Considering Safety Issues. In Proceedings of the ICHS2007—International Conference on Hydrogen Safety, San Sebastian, Spain, 11–13 September 2007.

19.　Pasman, H.J.; William, J.; Rogers, W.J. Risk assessment by means of Bayesian networks: A comparative study of compressed and liquefied H2 transportation and tank station risks. *Int. J. Hydrogen Energy* **2012**, *37*, 17415–17425. [CrossRef]

20.　Kim, Y.S.; Kim, S.S.; Choe, B.H. The Role of Hydrogen in Hydrogen Embrittlement of Metals: The Case of Stainless Steel. *Metals* **2019**, *9*, 406. [CrossRef]

21.　Fu, L.; Fang, H. Formation Criterion of Hydrogen-Induced Cracking in Steel Based on Fracture Mechanics. *Metals* **2018**, *8*, 940. [CrossRef]

22.　Valenti, G. Hidrogen liquefaction and liquid hydrogen storage. *Compend. Hydrog. Energy* **2016**, *2*, 27–51.

23.　Michel, F.; Fieseler, H.; Allidieres, L. Liquid Hydrogen Technologies for Mobile Use. In Proceedings of the WHEC 16, Lyon, France, 13–16 June 2006.

24.　Schlapbach, L.; Züttel, A. Hydrogen-storage materials for mobile applications. In *Materials for Sustainable Energy*; Dusastre, V., Ed.; Nature Publishing Group: London, UK, 2010; pp. 265–270.

25.　Bossel, U.; Eliasson, B.; Taylor, G. The future of the hydrogen economy bright or bleak? In Proceedings of the Fuel Cell Seminar, Miami Beach, FL, USA, 3–7 November 2003; pp. 367–382.

26.　National Renewable Energy Laboratory. *HSCoE Final Report Executive Summary*; U.S. Department of Energy: Golden, CO, USA, 2010.

27.　O'Hayre, R.; Cha, S.; Colella, W.; Prinz, F. *Fuel Cell Systems Fundamentals*, 2nd ed.; Wiley: Hoboken, NJ, USA, 2009; ISBN-13 978-0470258439.

28.　Perry, R.H.; Green, D.W.; Maloney, J.O. *Perry's Chemical Engineers' Handbook*, 7th ed.; McGraw-Hill: New York, NY, USA, 1997; ISBN 0-07-049841-5.

29.　Dwivedi, S.K.; Vishwakarma, M. Hydrogen embrittlement in different materials: A review. *Int. J. Hydrogen Energy* **2018**, *43*, 21603–21616. [CrossRef]

30.　Humpenoder, J. Gas permeation of fibre reinforced plastics. *Cryogenics* **1998**, *38*, 143–147. [CrossRef]

31.　Song, W.; Du, J.; Xu, Y.; Long, B. A study of hydrogen permeation in aluminum alloy treated by various oxidation processes. *J. Nucl. Mater.* **1997**, *246*, 139–143. [CrossRef]

32.　Van Deventer, E.H.; Maroni, V.A. Hydrogen permeation characteristics of some austenitic and nickel-base alloys. *J. Nucl. Mater.* **1980**, *92*, 103–111. [CrossRef]

33.　Schefer, R.W.; Hout, W.G.; San Marchi, C.; Chernicoff, W.P.; Englom, L. Characterization of leaks from compressed hydrogen dispensing systems and related components. *Int. J. Hydrogen Energy* **2006**, *31*, 1247–1260. [CrossRef]

34. Schultheiß, D. Permeation Barrier for Lightweight Liquid Hydrogen Tanks. Ph.D. Thesis, Universitat Augsburg, Augsburg, Germany, 16 April 2007.

35. Kirkaldy, J.; Young, D. *Diffusion in the Condensed State*; The Institute of Metals: London, UK, 1987; ISBN 0904357872.

36. Steward, S.A. *Review of Hydrogen Isotope Permeability Through Materials*; Lawrence Livermore National Laboratory: Berkeley, CA, USA, 1983.

37. Suda, H.; Yamauchi, H.; Uchimaru, Y.; Fujiwara, I.; Haraya, K. Preparation and gas permeation properties of silicon carbidebased inorganic membranes for hydrogen separation. *Desalination* **2006**, *193*, 252–255. [CrossRef]

38. European Union. Commission Regulation (EU) No 406/2010 of 26 April 2010 implementing Regulation (EC) No 79/2009 of the European Parliament and of the Council on type-approval of hydrogen-powered motor vehicle. Available online: https://eur-lex.europa.eu/LexUriServ/LexUriServ.do?uri=OJ:L:2010:122:0001:0107: EN:PDF (accessed on 9 May 2019).

39. Adams, P.; Bengaouer, A.; Cariteau, B.; Molkov, V.; Venetsanos, A. Allowable hydrogen permeation rate from road vehicles. *Int. J. Hydrogen Energy* **2011**, *36*, 2742–2749. [CrossRef]

40. Waterland, L.R.; Powars, C.; Stickes, P. *Safety Evaluation of the FuelMaker Home Refueling Concept Final Report*; National Renewable Energy Laboratory: Golden, CO, USA, 2005.

41. Mitlitsky, F.; Weisberg, H.A.; Myers, B. *Vehicular Hydrogen Storage Using Lightweight Tanks*; Lawrence Livermore National Laboratory: Berkeley, CA, USA, 2000.

42. Moretto, P.; Acosta-Iborra, B.; Baraldi, D.; Galassi, M.; De Miguel, N.; Ortiz Cebolla, R. Onboard Compressed Hydrogen Storage: Fast filling. In Proceedings of the IA HySafe and JRC IET Workshop, Research Priorities and Knowledge Gaps in Hydrogen Safety, Berlin, Germany, 16–17 October 2012.

43. *ISO 11119-3:2002 Gas Cylinders of Composite Construction—Specification and Test Methods—Part 3: Fully Wrapped Fibre Reinforced Composite Gas Cylinders with Non-Load-Sharing Metallic or Non-Metallic Liners*; International Standards Organization: Geneva, Switzerland, 2002.

44. Echtermeyer, A.T.; Lasn, K. *Myers, B. Safety Factors and Test Methods for Composite Pressure Vessels*; European Union: Brussels, Belgium, 2013.

45. DNV-OS-C50:2013. *Composite Components*; DET NORSKE VERITAS AS: Høvik, Norway, 2013.

46. Aigueperse, J.; Mollar, P.; Devilliers, D.; Chemla, M.; Faron, R.; Romano, R.; Cuer, J. Fluorine Compounds, Inorganic. In *Ullmann's Encyclopedia of Industrial Chemistry*; Wiley: Hoboken, NJ, USA, 2012; Volume 15.

47. Hales, T.; Ferguson, S. A Formulation of the Kepler Conjecture. *Discret. Comput. Geom.* **2006**, *36*, 21–69. [CrossRef]

48. Hales, T.; Adams, M.; Bauer, G.; Dang, T.; Harrison, J.; Hoang, L.; Zumkeller, R. A Formal Proof of the Kepler Conjecture. *Forum Math.* **2017**, *5*, 1–29. [CrossRef]

49. Silbert, L. Jamming of frictional spheres and random loose packing. *Soft Matter* **2010**, *6*, 2918–2924. [CrossRef]

50. Dong, K.; Yang, R.; Zou, R.; Yu, A. Role of Interparticle Forces in the Formation of Random Loose Packing. *Phys. Rev. Lett.* **2006**, *96*, 145505. [CrossRef]

51. Onoda, G.; Liniger, E. Random Loose Packings of Uniform Spheres and the Dilatancy Onset. *Phys. Rev. Lett.* **1990**, *64*, 2727–2730. [CrossRef]

52. Scott, G.; Kilgour, D. The density of random close packing of spheres. *J. Phys. D Appl. Phys.* **1969**, *2*, 863–869. [CrossRef]

53. Scott, G. *Packing of Spheres*; Nature Publishing Group: London, UK, 1960; pp. 908–909.

54. Donev, A. Improving the Density of Jammed Disordered Packings Using Ellipsoids. *Science* **2004**, *303*, 990–993. [CrossRef]

55. Man, W.; Donev, A.; Stillinger, F.; Sullivan, M.; Russel, W.; Heeger, D.; Chaikin, P. Experiments on Random Packings of Ellipsoids. *Phys. Rev. Lett.* **2005**, *94*, 198001-1–198001-4. [CrossRef]

56. Pouliquen, O.; Nicolas, M.; Weidman, P. Crystallization of non-Brownian Spheres under Horizontal Shaking. *Phys. Rev. Lett.* **1997**, *79*, 3640–3643. [CrossRef]

57. Hyundai NEXO Press Kit. Available online: https://www.hyundai.news/eu/press-kits/0/NEXO/ (accessed on 19 February 2018).

58. Outline of the Mirai. Available online: https://www.toyota-europe.com/new-cars/mirai/index/specs (accessed on 19 February 2018).